Solvent Effects on the Low-Lying Excited States of a Model of Retinal

Aurora Muñoz Losa, Ignacio Fdez. Galván, M. Elena Martín, and Manuel A. Aguilar*

Departamento de Química Física, Facultad de Ciencias, Universidad de Extremadura, Avda de Elvas s/n, 06071 Badajoz, Spain

Received: December 29, 2005; In Final Form: May 30, 2006

The low-lying excited states of a solution in alcohol of a five-double-bond model of the rhodopsin protein chromophore, the protonated 11-*cis*-retinal Schiff base (PSB11), are studied theoretically. We combine a multireference perturbational treatment in the description of the solute molecule with molecular dynamics calculations in the description of the solvent. The geometry, charge distribution, and electronic spectra are strongly influenced by the solvent. The solvent shift values show a marked dependence on the use of relaxed geometries in solution and on the nature of the states involved in the excitation process. The dynamic correlation has a strong effect on the order of the excited states. In solution, the first two excited states almost become degenerate.

I. Introduction

Rhodopsin is a membrane protein located in rod dishes of vertebrates. Rod cells are responsible for the capacity for low light intensity vision. Rhodopsin contains a chromophore, 11-*cis*-retinal, bound to opsin through a Schiff base linkage with a lysine residue. With the absorption of one photon, rhodopsin undergoes isomerization of the 11-*cis*-retinal to the all-trans form in a very fast process that takes less than 200 fs.[1,2] This triggers the vision process. Even if, a priori, any double bond would be suitable to isomerize, the isomerization in rhodopsin only takes place around the C11−C12 double bond. This selectivity has its roots in the interactions between the chromophore and the protein pocket. These interactions are also responsible for the different absorptions that the same chromophore shows in different environments. Thus, the protonated 11-*cis*-retinal Schiff base chromophore of rhodopsin (PSB11) absorbs at 498 nm, whereas the same chromophore in bright light sensitive cone pigments absorbs between 360 and 600 nm. The interaction of the chromophore with the protein is also different from what occurs inside a solvent. For instance, the PSB11 absorption in methanol has been estimated[3] to be at 442 nm, showing a 50 nm blue shift from the natural situation. In addition, it has been observed that in methanol the isomerization process is 2 orders of magnitude slower, taking 10 ps for the transformation to the all-trans isomer.[4] In this case a transient fluorescent state is formed with a 3 ps fluorescence lifetime, whereas inside the protein this state fluoresces only for 50−60 fs.[5,6]

Precise knowledge of the behavior of these processes has long come predominantly from experiment, since theoretical chemistry did not have the required tools. The first theoretical studies were semiempirical and were performed before the crystallographic structure of rhodopsin was available.[7−10] A few years ago, the X-ray crystal structure of bovine rhodopsin[11,12] became available at a 2.8 Å resolution, giving one the opportunity to look inside the real isomerization mechanism and locate the residues and interactions that determine the isomerization process. Given that the first step of the isomerization process is the absorption of a photon, there is growing interest in the theoretical description of the electronic excitation of the $S_0 \rightarrow S_1$ transition and in the characterization of the chromophore geometry and its movements in vacuo, in solution, and inside the protein pocket.[13−27] Various studies[28−30] have shown that highly accurate quantum methods, such as complete active space with second-order perturbation theory (CASPT2) or second-order multireference perturbation theory (MRPT2), and very precise geometrical parameters must be used if one wants to obtain an adequate description of the chromophore spectra. Experimentally, a recent study of Andersen et al.[31] has provided the position of the absorption band of the retinal protonated Schiff base (PSB) in vacuo (610 nm). This information, together with the absorption data in different solvents[3], has for the first time provided accurate data about the magnitude of the solvent shift.

Our study is a first step toward understanding the spectra and isomerization process of PSB11 in methanol solution. We focus on the first event of the photochemical process, i.e., the vertical transition to the first excited states of a PSB model, taking into account interactions and conformational changes originated by the solvent. We shall describe the isomerization process in a later paper. Given the considerable chromophore size, if one wants to perform accurate calculations, such as with CASPT2//CASSCF or CASPT2//MP2 protocols (geometry optimization at the CASSCF or MP2 level and energy calculation at the CASPT2 level), it is customary to use reduced chromophore models. In our case, we use the tEtZtEt-nona-2,4,6,8-tetraenimine cation (Figure 1), which reproduces the most important structural features of the real system. In particular we address the solvent's influence on the solute geometry, transition energy, and nature of the states involved. Effects of the calculation level on the geometry and properties of the system are also analyzed. A few studies of similar chromophores in the presence of methanol can be found in the literature. For instance, Gao et al.[32] performed a detailed study of the opsin shift for the bacteriorhodopsin chromophore, making CIS/3-21 QM/MM calculations for the study of the chromophore in methanol solution. Andruniów et al.[33] used a higher level of ab initio calculation (CASPT2//CASSCF) to describe PSB11

* Author to whom correspondence should be addressed. E-mail: maguilar@unex.es.

10.1021/jp057563n CCC: $33.50
Published on Web 08/22/2006

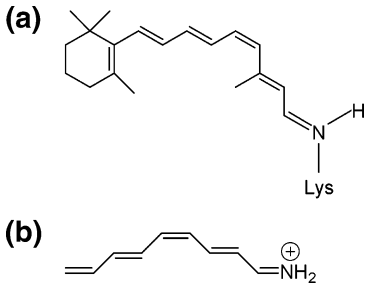

Figure 1. (a) 11-Cis isomer of the retinal protonated Schiff base (PSB11). (b) M1 model tEtZtEt-nona-2,4,6,8-tetraenimine cation ($C_9H_{10}-NH_2^+$).

in the presence of an optimized methanol cluster. Only one solvent configuration is considered, and as a consequence, thermal and entropic contributions are not taken into account.

The paper is organized as follows: Section II gives a description of the averaged solvent electrostatic potential from molecular dynamics (ASEP/MD) method and its main characteristics. Section III outlines the computational details of the calculations. Section IV reports the most significant results obtained in the study, and finally section V gives a summary and the conclusions.

II. Method

The solvent effects were taken into account using the ASEP/MD method. This is a quantum mechanics/molecular mechanics (QM/MM) method that makes use of the mean field approximation. Its main characteristics have been described elsewhere.[34−38] Here, we shall detail only those points pertinent to the current study.

The determination of solvent shifts with the ASEP/MD method involves two self-consistent processes. In the first, the solvent structure and the charge distribution and geometry of the solute become mutually equilibrated. In the second, the solvent electron polarization responds to the changes in the solute charge distribution originating from the electron transition.

To obtain the energy and wave function of the solute and the solvent structure around it, ASEP/MD combines QM and MM techniques, with the particularity that full QM and MM calculations are alternated and not simultaneous. During the MD simulations, the solvent molecules are represented with rigid intramolecular geometries so that no intramolecular force terms are needed.

The solute wave function is obtained by solving the Shrödinger equation

$$(\hat{H}_{QM} + \hat{H}^{elect}_{QM/MM} + \hat{H}^{vdw}_{QM/MM})|\psi\rangle = E|\psi\rangle \quad (1)$$

with

$$\hat{H}^{elect}_{QM/MM} = \int d\mathbf{r}\, \hat{\rho} V_{ASEP}(r) \quad (2)$$

and

$$V_{ASEP}(r) = \langle \hat{V}_s(r,X)\rangle \quad (3)$$

where $\hat{H}^{vdw}_{QM/MM}$ is the Hamiltonian for the van der Waals interaction, in general being represented by a Lennard-Jones potential, and $V_{ASEP}(r)$ is the averaged electrostatic potential generated by the solvent that in general depends on the solute state and that can be represented through a set of point charges $\{q_i\}$. Technical details about the determination of the number, position, and values of the charges can be found in refs 34−35. Brackets indicate a statistical average over the solvent configurations X obtained in the MD calculation. Finally, $\hat{\rho}$ is the density charge operator of the solute.

The process finishes when convergence in the solute point charges and in the solute energy is reached. The point charges representing the chromophore molecule during the MD simulation were obtained from the in solution solute molecule wave function, eq 1, by using the charges from electrostatic potential, grid (CHELPG) method.[39,40] To optimize the geometry of the molecule in solution we used a technique described in a previous paper[41] based on the use of the free-energy gradient method.[42−44]

When the interest is in studying electronic transitions, it becomes necessary to perform an additional self-consistent process during the calculation of the ASEP. The solvent structure and solute geometry obtained in the first self-consistent process are used to couple the quantum mechanical solute and the electron polarization of the solvent. To this end, we assigned a molecular polarizability to every methanol molecule, located at its center of mass, and simultaneously replaced the effective methanol charge distribution used in the MD calculation by the ab initio gas-phase values of the solvent molecule (0.290498, −0.690418, and 0.423032 e for CH_3, O, and alcoholic H, respectively). The dipole moment induced on each solvent molecule is a function of the dipole moments induced on the rest of the molecules and of the solute charge distribution, and hence the electrostatic equation has to be solved self-consistently. The process finishes when convergence in the solute and solvent charge distribution is reached. During the electron transition we apply the Franck−Condon principle, considering as fixed the solute geometry and the solvent structure around it. However, the electron degrees of freedom of the solvent are allowed to respond to the change in the solute charge distribution.

The total energy of the system (quantum solute + polarizable solvent) is obtained as[45,46]

$$U = U_{qq} + U_{pq} + U_{pp} + U_{\rho q} + U_{\rho p} + U^{solute}_{dist} + U^{solvent}_{dist} \quad (4)$$

Here, q refers to the permanent charges of the solvent molecules, p to the solvent-induced dipoles, and ρ is the solute charge density. The last two terms in eq 4 are the distortion energies of the solute and solvent, i.e., the energy spent in polarizing them.

The different contributions are[47]

$$U_{qq} = \frac{1}{2}\sum_i q_i V_i^q$$

$$U_{pq} = -\sum_i \vec{p}_i \cdot \vec{E}_i^{\,q}$$

$$U_{pp} = -\frac{1}{2}\sum_i \vec{p}_i \cdot \vec{E}_i^{\,p}$$

$$U^{solvent}_{dist} = \sum_i \frac{\vec{p}_i \vec{\alpha}_i^{-1} \vec{p}_i}{2} = \frac{1}{2}\sum_i \vec{p}_i \cdot \vec{E}_i = \frac{1}{2}\sum_i \vec{p}_i [\vec{E}_i^{\,q} + E_i^{\rho} + \vec{E}_i^{\,p}] = -\frac{1}{2}U_{pq} - U_{pp} - \frac{1}{2}U_{\rho p} \quad (5)$$

$$U_{\rho q} = \sum q_i V_i^{\rho}$$

$$U_{\rho p} = \sum p_i \vec{E}_i^{\,\rho}$$

$$U^{solute}_{dist} = \langle \Psi | H_{QM} | \Psi \rangle - \langle \Psi^0 | H_{QM} | \Psi^0 \rangle$$

where Ψ and Ψ^0 are the in solution and in vacuo solute wave functions, respectively, and V_i^{ρ} and V_i^{q} are the electrostatic potentials generated by the solute charge distribution and by the permanent charges of the solvent, respectively. The electric field generated by the solute, solvent permanent charges, and solvent-induced dipoles are, respectively, $\vec{E}_i^{\rho}$, $\vec{E}_i^{q}$, and $\vec{E}_i^{p}$. The terms that involve the solute molecule are calculated quantum-mechanically. The final expression for the total energy of the system is

$$U = U_{qq} + \frac{1}{2}U_{pq} + U_{\rho q} + \frac{1}{2}U_{\rho p} + U_{\text{dist}}^{\text{solute}} \qquad (6)$$

Once the solvation energy has been calculated for the ground and excited states, the solvent shift can be obtained as the difference

$$\delta = U_{\text{ex}} - U_{\text{g}} = \frac{1}{2}\delta_{pq} + \delta_{\rho q} + \frac{1}{2}\delta_{\rho p} + \delta_{\text{dist}}^{\text{solute}} \qquad (7)$$

The term δ_{qq} cancels out because, in vertical transitions where the Franck−Condon approximation is applicable, the U_{qq} term takes the same value in both the ground and the excited state; i.e., the equilibrium solvent structure is only calculated for the ground state. From a practical point of view that means that the first self-consistent process (with or without geometry optimization) is carried out just for the ground state. However, the second cyclic process that permits the response of the electron degrees of freedom of the solvent is carried out for both the ground and the excited states.

III. Computational Details

The ASEP-MD method was used to study the $^1(\pi \rightarrow \pi^*)$ transition in a five-double-bond model of the PSB11 of retinal. The ground and excited states of the PSB11 model were described using the complete active space self-consistent field (CASSCF)[48] level of theory. To improve the energy results, a dynamic correlation energy was included with second-order perturbation theory (CASPT2).[49−50] All electrons of the π skeleton were included in the active space, which was spanned by all the configurations arising from 10 valence π electrons in 10 orbitals (10e, 10o). In all calculations, the split-valence 6-31G* basis set was employed. This has been widely used in studies of the photophysics of different models of PSB11.

The MD simulations were carried out using the program MOLDY.[51] This program considers the system to be an assemblage of rigid molecules and employs a modification of the Beeman algorithm proposed by Refson.[52] The simulation had one chromophore molecule and 630 methanol molecules contained at a fixed intramolecular geometry in a cubic box of 35 Å. No counterion was included. Previous studies of Rajamani and Gao[32] and Röhrig et al.[53] using chloride as a counterion find that, because of the large dielectric screening effects of methanol, the effect of the counterion on the structure and spectra of the solvent is minimal. This has been corroborated by experiments showing that the position of the chromophore absorption band in polar solvents is not affected by the nature of the counterion.[54] The solute parameters were obtained by combining Lennard-Jones interatomic interactions[55] with electrostatic interactions. Periodic boundary conditions were applied, and spherical cutoffs were used to truncate the PSB11 model and methanol interactions at 9 Å. The electrostatic interaction was calculated with the Ewald method. The temperature was fixed at 298 K using the Nosé−Hoover[56] thermostat. Each simulation was run for 150 000 time steps, where 50 000 were for equilibration and 100 000 were for production. A time step of 0.5 fs was used.

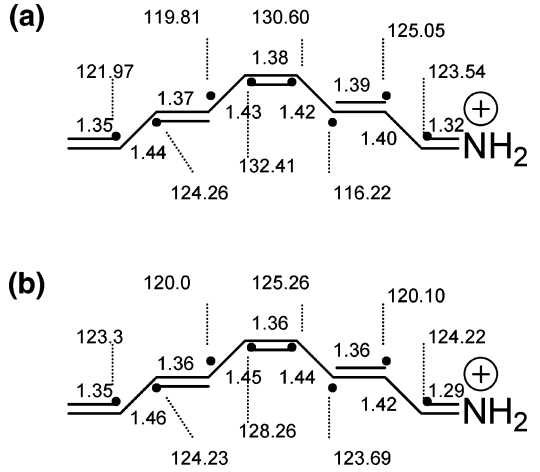

Figure 2. Geometry parameters for the in vacuo optimized geometries (distances in Å): (a) MP2, (b) CASSCF.

During the ASEP/MD cycle, the quantum calculations were performed at the CASSCF or MP2 level of theory using the GAUSSIAN98 package[57] of programs. Once the solute−solvent structure had been obtained, the electron transition was calculated at the CASSCF level (CASSCF//CASSCF and CASSCF//MP2 calculations). However, it is known[58] that to correctly describe electron transitions in conjugated molecules one must include the dynamic correlation contribution. Hence, once we had obtained the solvent structure around the solute, we used the CASPT2 method included in MOLCAS-5[59] to recalculate the transition energies and solvent shift values (CASPT2//CASSCF and CASPT2//MP2 calculations).

Independently of the level of the QM calculation, all ASEP/MD calculations were run for 10 cycles. The final results were obtained by averaging the last five ASEP/MD cycles (250 ps).

IV. Results

In Vacuo Study. In this section we shall present the results for the first two transitions of the UV−vis spectra of the tEtZtEt-nona-2,4,6,8-tetraenimine cation ($C_9H_{10}-NH_2^+$). This cation, hereafter termed M1, has been widely used as a model of PSB11 because it reproduces important structural features of the real system, in particular, the 11-cis double bond of PSB11, the polyeniminium residues ($-CH=NH_2^+$), and the remaining unsaturated chain with the exception of the β-ionone ring replaced by a hydrogen atom. With this model all the conjugated double bonds of the aliphatic chain are included. As the PSB11 ionone ring inside the protein is highly twisted (ca. 60°) with respect to the molecular plane,[11] it is expected to show a smaller conjugation with the rest of the polyene chain. In fact, M1 provides a model for a twisted (90°) PSB11 chromophore.

As a first step, the geometry of the system in the ground state was optimized in vacuo at the CASSCF multiconfigurational and MP2 levels of calculation. All geometrical variables were allowed to relax.

In vacuo and at the CASSCF level, the molecule shows a totally planar structure, and the intramolecular parameters are in full agreement with other theoretical studies.[60] Figure 2b shows these parameters. As in similar oligomers, a clear alternation can be seen between single and double bonds. The bond length alternation (BLA) smooths out as the iminium residue is approached. The BLA value, calculated as the sum of all formal single-bond lengths minus the sum of all formal

double-bond lengths, is 0.34 Å. The vertical transition $^1(\pi \rightarrow \pi^*)$ from the relaxed ground state involves 3.55 eV at the CASSCF//CASSCF level and 2.56 eV at the CASPT2//CASSCF level (Table 3). Clearly, the inclusion of the dynamic correlation component is compulsory if one wants to obtain an accurate transition energy. Our results are almost coincident with those obtained by González-Luque et al.[61] who employed the same model and level of calculations but a somewhat fuller basis set that includes supplementary diffuse functions for a better description of the Rydberg states.

Next, we repeated the estimation of the $^1(\pi \rightarrow \pi^*)$ vertical transition energy at the CASSCF and CASPT2 levels but now performing an MP2 geometry optimization of the M1 model (CASSCF//MP2 and CASPT2//MP2 calculations, respectively). The results showed that the MP2-optimized geometry is also a totally planar structure but appreciably different from that obtained at the CASSCF level. There are smaller differences between single and double bonds (the BLA is 0.20 Å), and the alternation between single and double bonds smooths out faster than for the CASSCF geometry as the iminium residue is approached (Figure 2a). This variation in geometry leads to an energy difference of ca. 7 kcal/mol in the vertical transition energy compared to the CASSCF-optimized geometry energy (3.23 eV for CASSCF//MP2). At the CASPT2//MP2 level of calculation, the vertical transition energy is 2.40 eV. These results agree with those obtained by Schreiber and co-workers[62,63] who reported values of 3.30 and 2.45 eV for the same transition at the CASSCF and CASPT2 levels of calculation. Those authors used an almost planar B3LYP/6-31G** optimized geometry and an active space of 10 electrons in 10 π-orbitals as well for the multiconfigurational calculation, performing state averaging for the two states considered. (Our calculation refers, unless otherwise specified, to pure root calculations, both in vacuo and in solution.)

Although there are no experimental data for the UV−vis absorption spectra of PSB11 in vacuo,[66] a precise estimate of the maximum's position is possible. Recently, it has been determined that the maximum of the band in the all-trans photoproduct (PSBT) appears at 2.03 eV.[31] High-level quantum calculations (Cembran et al.[28]) of PSB11 and PSBT in vacuo as well as experimental data in different solvents[3] do not show any significant differences between the absorption spectra of PSB11 and PSBT. Hence one can assume that the maximum of the absorption band of PSB11 must also be close to 2.03 eV. Taking this value as reference, it seems clear that the CASPT2//MP2 calculation yields better values than CASPT2//CASSCF. In fact, it is known that CASSCF geometries tend to overestimate the BLA[64] and that this factor has a significant influence on the S_1 vertical excitation energy, a fact previously noted by Hufen et al.[29] Our best CASPT2//MP2 calculation overestimates the transition energy by about 0.37 eV due probably to the absence of the β-ionone ring in the model. In fact, this difference is consistent with the hypsochromic shift of 0.3 eV estimated by Wanko et al.[30] when the β-ionone ring of the complete chromophore is forced to have a torsion angle of 90° with respect to the original in vacuo torsion of 33° calculated at the B3LYP level.

Another point to consider is the nature of the electron states involved in the vertical transition. It is common to identify the first and second excited states in PSBs as $1B_u$-like and $2A_g$-like, or ionic and covalent states, respectively. The calculated oscillator strength for the $S_0 \rightarrow S_1$ in vacuo transition was 1.15. This high value indicates that the transition was to an allowed $1B_u$-like excited state.

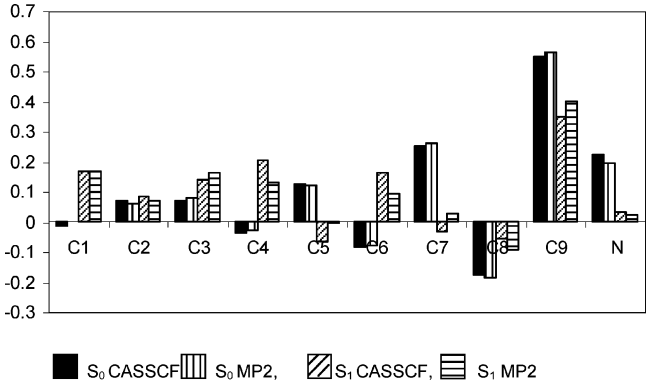

Figure 3. CASSCF calculated electronic charge distribution for the ground and first excited states optimized in a vacuum at the MP2 and CASSCF levels.

TABLE 1: In Vacuo Dipole Moments (D) and in Solution Dipole Moment Increments (D) for the Ground State and the Ionic and Covalent Excited States Calculated at the CASSCF Level

geometry	S_0[a]	ionic[a]	covalent[a]	$\Delta\mu$ (S_0)[b]	$\Delta\mu$ (ionic)[b]	$\Delta\mu$ (covalent)[b]
CASSCF(vac)	13.9	1.7	11.2			
CASSCF(sol)				5.1	8.8	5.9
MP2(vac)	13.7	0.9	10.0	5.9	5.5	9.05
MP2(sol)				5.7	8.5	10.0

[a] In vacuo. [b] In solution.

In Figure 3, the charge distribution representation for the S_0 and S_1 states calculated with CHELPG at the CASSCF level with CASSCF- and MP2-optimized geometries allows one to analyze the chromophore electron distribution and also the nature of their wave functions. As one can see, S_0 shows an electron deficit located mainly in the C7−N chain fragment and more specifically in the C9−N bond. On the contrary, in S_1 there is no such marked charge location, with its distribution being smoother. During the excitation, almost 40% of the positive charge moves from its position in S_0 to the backbone chain. As a conclusion, it can be noted that, in vacuo, S_0 is a charge-localized state, while S_1 has the charge distributed along the skeleton. These results agree with the situation in polyenes where, using valence bond terms, the ground state corresponds to a dot−dot (covalent) state while the in vacuo first excited state corresponds to a hole−pair (ionic) excitation. Given that S_0 and S_1 present two very different distributions, a notable dipole moment difference can also be expected. This difference was estimated at 12.20 or 12.80 D at the CASSCF or MP2 levels of optimization, respectively (Table 1). The ground state has the largest dipole moment because of its positive charge accumulated in the C7−N fragment. González-Luque et al.[61] obtained similar results in studying the S_0 and S_1 (at the FC point) charge distribution in a similar chromophore model and in vacuo conditions (14.0 D).

Finally we estimated the $S_0 \rightarrow S_2$ transition energy to be 4.13 or 3.16 eV at the CASSCF//MP2 and CASPT2//MP2 levels, respectively, the value of the dipole moment of S_2 being 9.10 D. The calculated oscillator strength for the in vacuo transition from S_0 to S_2 was 0.09. This value indicates that this in vacuo transition is to an optically forbidden state, where the charge is mainly localized in the C7−N fragment. Both ground and second excited states can be considered to be covalent or charge-localized states.

In Solution Study. In this section we shall present the results for the solvent influence on the two lowest vertical transitions

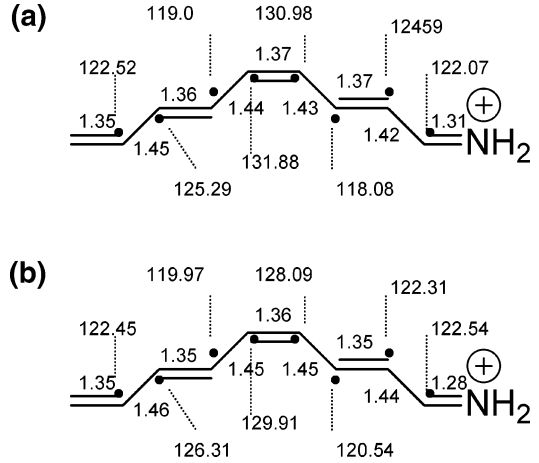

Figure 4. Geometry parameters for the in solution optimized geometries (distances in Å): (a) MP2, (b) CASSCF.

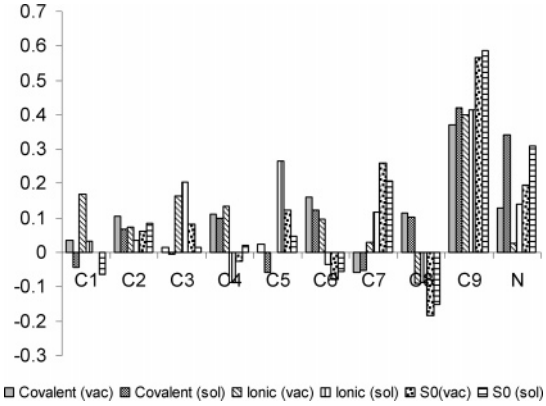

Figure 5. Electronic charge distribution for the first excited states optimized in solution at the MP2 level.

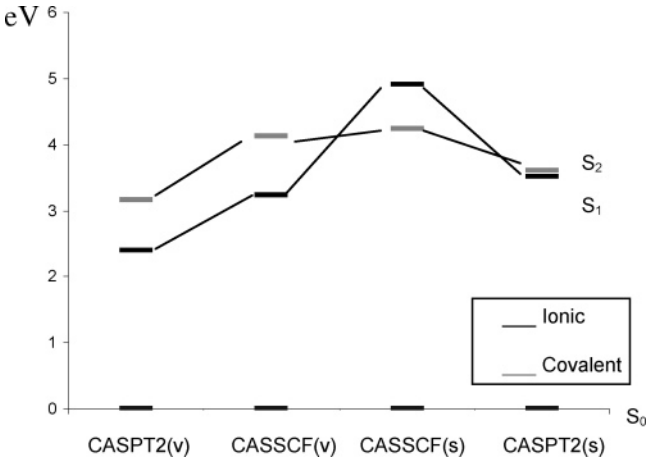

Figure 6. Computed CASSCF//MP2(sol) and CASPT2//MP2(sol) vertical electronic transitions for the ionic and covalent low-lying excited states.

of the M1 model for the PSB11 cation. For the second excited state the state average option was selected, giving equal weight to the two upper roots to avoid convergence problems. Multistate CASPT2 calculations were performed to correct the energies by including the effect of the dynamical correlation. No differences were found with the CASPT2 results, so hereafter this kind of improvement will be referred to as the CASPT2 calculations.

We begin with the analysis of the geometric changes induced by the solvent on the ground state (Figure 4). As expected, interaction with the solvent causes some variations in the C−C bond lengths in comparison with the bond-length alternation in vacuo: Double bonds become shorter, and single bonds become longer. This trend is more evident as one approaches the Schiff base nitrogen and when one uses CASSCF geometries. The BLA values are now 0.39 and 0.29 Å at the CASSCF and MP2 levels, respectively.

In the FC region and at the CASSCF//MP2 level of calculation, the solvent produces an inversion in the stability of the two excited states from the in vacuo situation, with the so-called covalent state becoming lower in energy. This is confirmed in the value of the oscillator strength which is 0.01 for the S_0-S_1 transition and about 1.0 for the S_1-S_2 transition. A low value of this magnitude indicates that the studied transition involves states of similar nature that, as was concluded above from studying the solute charge distribution in solution, locate the positive charge mainly on the iminium residue. This was corroborated by the dominant configuration participating in each state, i.e., doubly excited for S_1 and a highest occupied molecular orbital−lowest unoccupied molecular orbital (HOMO−LUMO) transition for S_2. A similar inversion in the order of the exited states has been found by Ferré et al.[17] in a study of a similar but methylated model in the presence of Glu113. The situation changed when the energies are recomputed at the CASPT2 level. In this case, the ionic state was again the lowest excited state, with the two excited roots being very close in energy (Figure 6). Hence, to make the description of the in solution results clearer, hereafter we will refer to the excited states as ionic (HOMO−LUMO transition) and covalent (doubly excited transition) states, corresponding to the $1B_u$-like and $2A_g$-like in vacuo states, respectively.

As expected, the solvent tends to localize the positive charge on the iminium residue. Figure 5 shows the in solution and in vacuo CHELPG charges for the ground and two first excited states of the M1 model, when the ground-state geometry was optimized at the MP2 level of calculation. As one can see from Table 1, the solvent perturbation increases the dipole moment notably, by around 40% in the ground state. This result is independent of the use of in vacuo or in solution optimized geometries. In comparison to the ground state, excited states undergo a much more dramatic increase in their dipole moments as a consequence of the solvent's influence. (The dipole increments were calculated as the difference between the corresponding dipolar components.) As can be observed in Figure 5, the solvent favors charge-localized states, and for all the states there exists an accumulation of positive charge on the right side of the molecule when the solvent effect is taken into account. This effect is estimated at around 18% for the ground and ionic excited states and about 30% for the covalent excited state.

The total value of the solvent shift and its different components, calculated according to eq 7, for the transitions $S_0 \rightarrow$ ionic state and $S_0 \rightarrow$ covalent state are given in Table 2. The first column corresponds to the solvent shift due to the electrostatic interaction between the solute charge distribution and the permanent charges of the solvent. The second and third columns correspond to the interaction between the induced solvent dipoles and the solute charge distribution and permanent solvent charges, respectively. The fourth column is the contribution of the solute distortion energy. The total solvent shift is given in the last column. (CASPT2 values are included in brackets.)

In the transition to the ionic excited state, the solvent shift has a different predominant contribution depending on the kind of calculation. This behavior is consistent with the charge

TABLE 2: Solvent Shift (eV) and Its Components (kcal/mol) Calculated at the CASSCF Level

	$\delta_{q\rho}$	$^1/_2\,\delta_{p\rho}$	$^1/_2\,\delta_{pq}$	δ_{dist}^{solute}	$\delta^{a,b}$ (eV)
			$S_0 \rightarrow$ Ionic State		
CASSCF//MP2(vac)	22.7 ± 3.07	6.5 ± 0.62	-0.6 ± 0.22	5.8 ± 1.06	1.49 ± 0.12 [0.87 ± 0.01]
CASSCF//MP2(sol)	14.8 ± 1.36	5.6 ± 0.23	-0.2 ± 0.12	18.4 ± 0.56	1.67 ± 0.04 [1.11 ± 0.01]
CASSCF//CASSCF(sol)	12.7 ± 1.08	2.8 ± 0.17	-1.1 ± 0.62	23.9 ± 0.84	1.66 ± 0.07 [1.25 ± 0.02]
			$S_0 \rightarrow$ Covalent State		
CASSCF//MP2(sol)	1.2 ± 0.12	0.4 ± 0.05	-0.02 ± 0.02	3.6 ± 0.34	0.23 ± 0.01 [0.45 ± 0.02]

[a] Values in parentheses calculated at CASPT2 level. [b] Solvent shift calculated as energy difference between the transition in solution and the same transition in the gas phase.

TABLE 3: In Vacuo and in Solution Transition Energies (in eV) and Oscillator Strength Calculated at Different Levels

	$S_0 \rightarrow$ ionic		$S_0 \rightarrow$ covalent	
	vacuum	solution	vacuum	solution
CASSCF//CASSCF(sol)	3.55	5.22	4.61	4.62
CASPT2//CASSCF(sol)	2.56	3.82	3.58	3.78
CASSCF//MP2(sol)	3.23	4.90	4.13	4.22
CASPT2//MP2(sol)	2.40	3.51	3.16	3.61
experimental (PSB11)	2.03[a]	2.79[b]		
	Oscillator Strength			
CASPT2//MP2(sol)	1.15	1.00	0.09	0.01

[a] Reference 31. [b] Reference 3.

distribution changes that take place during the solvation process. Thus, for the CASSCF//MP2(vac) calculation the largest contribution comes from the solute−solvent electrostatic interaction, with the distortion component being somewhat lower but also positive. In this case, the difference between the energy costs for the polarization of the excited and ground states is estimated at around 5.8 kcal/mol; i.e., the excited state distorts its electron distribution to a greater extent than the ground state given the proportionally greater increment of its dipole moment. Consequently the energy spent in this distortion is greater for the excited state. Nevertheless, due to the fact that the ground and ionic excited states have very different dipole moments in solution, their interaction energies with the solvent (mainly with the solvent permanent charges) are also very different. For this reason, the corresponding components make important contributions to the solvent shift. When the evolution of these components is observed in Table 2, it can be noted that as one moves toward the calculations where the in solution geometry was allowed to relax and the ionic excited state dipole moment became greater, there exists an inversion of the weight of the contribution to the final solvent shift value. Taking into account that the increment of the dipole moment for the ground state is practically independent of the level of calculation, changes in the value of the solvent shift components must be mainly the result of changes in the charge distribution of the ionic excited state. Thus, as $\Delta\mu$ for the excited state becomes greater, the solute−solvent interaction energy becomes higher and more similar to that calculated for the ground state, resulting in a decrease of $\delta_{q\rho}$ and $\delta_{p\rho}$. With regard to the distortion component and in accordance with the previous conclusion, a greater increment of the excited-state dipole moment in solution leads to a greater value of the distortion energy, which, compared with an almost constant value for the corresponding energy for the ground state, gives rise to an increment in this component. Final values for the solvent shift are given in the last column. The CASSCF//CASSCF(sol) and CASSCF//MP2(sol) calculations give similar results for the solvent shift, with the values of their components being consistent with the above argument.

The calculation performed using the in vacuo MP2 geometry was very useful to better understand the nature of the solvent shift. The solvent shift is affected non-negligibly by the geometry relaxation during the solvation procedure. Its value increased by ca. 20%, 4.1 kcal/mol, when in solution optimized geometries were used. The distortion component, 18.4 kcal/mol, is the sum of two contributions, one corresponding to the distortion of the electron distribution and the other the energy spent in distorting the geometry. For the CASSCF//MP2(sol) calculation, the geometry relaxation contributes 7.2 kcal/mol to the total distortion energy, with the distortion of the electron distribution being obtained as the difference, yielding a value of 11.2 kcal/mol.

The nature of the solvent shift is completely different for the transition from S_0 to the covalent excited state. In this case, the largest contributions come from the distortion energy. This fact is related to the similar nature of these states. In solution, the initial and final states have similar dipole moment values, and hence the contributions of the electrostatic and polarization components are also similar, with the contribution of these components ($\delta_{q\rho}$ and $\delta_{p\rho}$) being relatively small. The solvent shift is mainly determined by the distortion energy. With regard to the distortion energy, the value given in Table 2 is consistent with the slightly greater $\Delta\mu$ shown by the covalent excited state in solution when compared with the ground state.

Another point to consider is the contribution of the solvent polarization to the total solvent shift. Perusal of Table 2 shows that the contribution of this component is important in the transition to the ionic excited state but almost negligible for the transition to the covalent one. The reason is that, in the latter case, the interaction between the solute charge distribution and the solvent-induced dipole moments in the ground and excited states cancel mutually. It is important to stress that in no case does this imply that the solvent polarization has no influence on the solute−solvent interaction energy. In fact, it represents almost 30% of the electrostatic contribution.

An important aspect to consider is whether a representation of the solvent polarization by effective charges (as is usual in most calculations) can reproduce the above results obtained using explicit polarizabilities. The solvent shift calculated for the transition to the ionic excited state when one uses effective fixed charges is 1.57 eV at the CASPT2//MP2 level. The difference is only 0.1 eV lower than the value obtained using explicit polarizabilities. Given the approximations introduced in the calculation of the solvent shift, it seems reasonable at a first approximation to neglect the effect of the explicit solvent polarization.

The experimental value of the solvent shift of PSB11 can be estimated to be about 0.76 eV (2.79 eV[3] minus 2.03[31] eV). We obtain for the M1 model 1.25 eV at the CASPT2//CASSCF level and 1.11 eV for the transition to the ionic excited state and 0.45 eV for the transition to the covalent one at the CASPT2//MP2 level.

The analysis of the results shows the strong influence that, in this system, the inclusion of the dynamical correlation has on the final value of the solvent shift. This situation is different

from that found in other systems, in acrolein, for instance, where the solvent shift is not affected by the inclusion of the dynamical correlation. This difference may be related to the different nature of the solvent shift. In acrolein the main component is the electrostatic interaction while in PSB11 it is the distortion component. Furthermore, although the BLA has a strong influence on the transition energies, it does not affect the solvent shift. Our calculation clearly overestimates the solvent shift. This overestimate can be understood by taking three considerations into account. First, M1 neglects the influence that the β-ionone ring and alkyl groups have on the solvation. Given the polar nature of the solvent and the apolar character of these groups, one expects that its inclusion would decrease the solute−solvent interaction energy and hence the solvent shift. Second, our calculations do not include the dispersion component contribution. This component gives rise to a red shift whose magnitude is very complicated to calculate. Third, M1 has a planar structure while PSB11 has a structure twisted around the central double bond.[65] The solvent shift is expected to be very sensitive to this aspect given the isomerization process undergone by the system and the known existence of a conical intersection during this event. Preliminary calculations performed in our laboratory show that the solvent shift decreases with increasing torsion angle around the C11−C12 double bond.

V. Conclusions

We have shown that the solvent has a strong influence on the structure, properties, and electronic spectra of a five-double-bond PSB11 model. Major variations in the ground-state geometry were found when optimization was performed in a methanol environment. The difference between single- and double-bond lengths increased compared with the in vacuo optimized geometry. This distortion led to a major localization of the positive charge in the iminium residue for the ground state and consequently a larger dipole moment value. When the $\pi \rightarrow \pi^*$ vertical transition was studied at the CASSCF//MP2 level in solution, a major change in the nature of the first excited states was observed. In this sense, the covalent state became lower in energy than the ionic one, with the order of the states being the inverse of that obtained with in vacuo conditions. Hence, the solvent changed the spectral order of the two lowest excited roots. Nevertheless, when the energies were recalculated at the CASPT2 level, the two lowest excited states became very close in energy and the ionic state returned to being the first excited root. This highlights the importance of including the effect of the dynamical correlation.

The calculated solvent shifts for the model studied were greater than the experimental value for the complete chromophore. This can be mainly attributed to the difference between the geometry of the model and that of the original system. As a consequence, the selected model does not adequately represent the solvation of the complete chromophore. Inside the protein, retinal shows a geometry slightly twisted around the C11−C12 bond, apart from the twist in the β-ionone ring with respect to the aliphatic chain. The M1 model, however, presents a planar structure both in vacuo and in solution. Nevertheless, this kind of structure has been widely used for many years in theoretical studies as the simplest models of the complete chromophore. Future efforts must be directed to a search for a better model, capable of reproducing the main characteristics of the PSB11 electron spectra in condensed media.

Acknowledgment. This research was sponsored by the Dirección General de Investigación Científica y Técnica (Grant No. CTQ2004-05680).

References and Notes

(1) Schoenlein, W.; Peteanu, L. A.; Mathies, R. A.; Shank, C. V. *Science* **1991**, *254*, 412−415.
(2) Wang, Q.; Schoenlein, R. W.; Peteanu, L. A.; Mathies, R. A.; Shank, C. V. *Science* **1994**, *266*, 422−424.
(3) Freedman, K. A.; Becker, R. S. *J. Am. Chem. Soc.* **1986**, *108*, 1245−1251.
(4) Kandori, H.; Katsuta, Y.; Ito, M.; Sasabe, H. *J. Am. Chem. Soc.* **1995**, *117*, 2669−2670.
(5) Kochendoerfer, G. G.; Mathies, R. A. *J. Phys. Chem.* **1996**, *100*, 14526−14532.
(6) Kandori, H.; Sasabe, H.; Nakanishi, K.; Yoshizawa, T.; Mizukami, T.; Shichida, Y. *J. Am. Chem. Soc.* **1996**, *118*, 1002−1005.
(7) Warshel, A.; Karplus, M. *J. Am. Chem. Soc.* **1974**, *96*, 5677−5689.
(8) Warshel, A. *Nature* **1976**, *260*, 679−683.
(9) Warshel, A.; Barboy, N. *J. Am. Chem. Soc.* **1982**, *104*, 1469−1476.
(10) Weiss, R.; Warshel, A. *J. Am. Chem. Soc.* **1979**, *101*, 6131−6133.
(11) Palczewslki, K.; Kumasaka, T.; Hori, T.; Behnke, C.; Motoshima, H.; Fox, B.; Le Trong, I.; Teller, D.; Okada, T.; Stenkamp, R.; Miyano, M. *Science* **2000**, *289*, 739−745.
(12) Teller, K.; Okada, T.; Cehnke, B.; Palczewki, K.; Stenkamp, R. *Biochemistry* **2001**, *40*, 7761−7772.
(13) Sugihara, M.; Buss, V.; Entel, P.; Elstner, M.; Frauenheim, T. *Biochemistry* **2002**, *41*, 15259−15266.
(14) Sugihara, M.; Entel, P.; Buss, V. *Phase Transitions* **2002**, *75*, 11−17.
(15) Yamada, A.; Kakitani, T.; Yamamoto, S.; Yamato, T. *Chem. Phys. Lett.* **2002**, *366*, 670−675.
(16) Rohrig, U.; Guidoni, L.; Rothlisberger, U. *Biochemistry* **2002**, *41*, 10799−10809.
(17) Ferre, N.; Olivucci, M. *J. Am. Chem. Soc.* **2003**, *125*, 6868−6869.
(18) Gascon, J. A.; Batista, V. S. *Biophys. J.* **2004**, *87*, 2931−2941.
(19) Vreven, T.; Morokuma, K. *Theor. Chem. Acc.* **2003**, *109*, 125−132.
(20) Vreven, T.; Bernardi, F.; Garavelli, M.; Olivucci, M.; Robb, M.; Schlegel, H. B. *J. Am. Chem. Soc.* **1997**, *119*, 12687−12688.
(21) Garavelli, M.; Vreven, T.; Celani, P.; Bernardi, F.; Robb, M.; Olivucci, M. *J. Am. Chem. Soc.* **1998**, *120*, 1285−1288.
(22) Ben-Nun, M.; Martinez, T. *J. Phys. Chem. A* **1998**, *102*, 9607−9617.
(23) La Penna, G.; Buda, F.; Bifone, A.; Groot, H. *Chem. Phys. Lett.* **1998**, *294*, 447−453.
(24) Garavelli, M.; Bernardi, F.; Robb, M.; Olivucci, M. *J. Mol. Struct. (THEOCHEM)* **1999**, *463*, 59−64.
(25) Molteni, C.; Franck, I.; Parrinello, M. *J. Am. Chem. Soc.* **1999**, *121*, 12177−12183.
(26) Hahn, S.; Stock, G. *J. Phys. Chem. B* **2000**, *104*, 1146−1149.
(27) Migani, A.; Sinicropi, A.; Ferré, N.; Cembran, A.; Garavelli, M.; Olivucci, M. *Faraday Discuss.* **2004**, *127*, 179−191.
(28) Cembran, A.; González-Luque, R.; Altoè, P.; Merchán, M.; Bernardi, F.; Olivucci, M.; Garavelli, M. *J. Phys. Chem. A* **2005**, *109*, 6597−6605.
(29) Hufen, J.; Sugihara, M.; Buss, V. *J. Phys. Chem. B* **2004**, *108*, 20419−20426.
(30) Wanko, M.; Hoffman, M.; Strodel, P.; Koslowski, A.; Thiel, W.; Neese, F.; Frauenheim, T.; Elstner M. *J. Phys. Chem. B* **2005**, *109*, 3606−3615.
(31) Andersen, L. H.; Nielsen, I. B.; Kristensen, M. B.; El Ghazaly, M. O. A.; Haacke, S.; Nielsen, M. B.; Petersen, M. Å. *J. Am. Chem. Soc.* **2005**, *127*, 12347−12350.
(32) Rajamani, R.; Gao, J. *J. Comput. Chem.* **2002**, *23*, 96−105.
(33) Andruniów, T.; Ferré, N.; Olivucci, M. *Proc. Natl. Acad. Sci. U.S.A.* **2004**, *101*, 17908−17913.
(34) Sánchez, M. L.; Aguilar, M. A.; Olivares del Valle, F. J. *J. Comput. Chem.* **1997**, *18*, 313−322.
(35) Sánchez, M. L.; Martín, M. E.; Aguilar, M. A.; Olivares del Valle, F. J. *J. Comput. Chem.* **2000**, *21*, 705−715.
(36) Muñoz Losa, A.; Fdez. Galván, I.; Martín, M. E.; Aguilar, M. A. *J. Phys. Chem. B* **2003**, *107*, 5043−5047.
(37) Sánchez, M. L.; Martín, M. E.; Fdez. Galván, I.; Olivares del Valle, F. J.; Aguilar, M. A. *J. Phys. Chem. B* **2002**, *106*, 4813−4817.
(38) Fdez. Galván, I.; Sánchez, M. L.; Martín, M. E.; Olivares del Valle, F. J.; Aguilar, M. A. *Comput. Phys. Commun.* **2003**, *155*, 244−259.
(39) Chirlian, L. E.; Francl, M. M. *J. Comput. Chem.* **1987**, *8*, 894−905.
(40) Breneman, C. M.; Wiberg, K. B. *J. Comput. Chem.* **1990**, *11*, 361−373.
(41) Fdez. Galván, I.; Sánchez, M. L.; Martín, M. E.; Olivares del Valle, F. J.; Aguilar, M. A. *J. Chem. Phys.* **2003**, *118*, 255−263.
(42) Okuyama-Yoshida, N.; Nagaoka, M.; Yamabe, T. *Int. J. Quantum Chem.* **1998**, *70*, 95−103.

(43) Okuyama-Yoshida, N.; Kataoka, K.; Nagaoka, M.; Yamabe, T. *J. Chem. Phys.* **2000**, *113*, 3519−3524.
(44) Hirao, H.; Nagae, Y.; Nagaoka, M. *Chem. Phys. Lett.* **2001**, *348*, 350−356.
(45) Gao, J. L. *J. Comput. Chem.* **1997**, *18*, 1061−1071.
(46) Thompson, M. A. *J. Phys. Chem.* **1996**, *100*, 14492−14507.
(47) Martín, M. E.; Muñoz Losa, A.; Fdez.-Galván, I.; Aguilar, M. A. *J. Chem. Phys.* **2004**, *121*, 3710−3716.
(48) Roos, B. O. In *Ab Initio Methods in Quantum Chemistry*; Lawley, K. P., Ed.; Wiley: New York, 1987; pp 399−446.
(49) Andersson, K.; Malmquist, P. A.; Roos, B. O. *J. Chem. Phys.* **1992**, *96*, 1218−1226.
(50) Malmquist, P. A.; Roos, B. O. *Chem. Phys. Lett.* **1989**, *155*, 189−194.
(51) Refson, K. *Comput. Phys. Commun.* **2000**, *126*, 310−329.
(52) Refson, K. *Physica B* **1985**, *131*, 256−266.
(53) Röhrig, U. F.; Guidoni, L.; Rothlisberger, U. *ChemPhysChem* **2005**, *6*, 1836−1847.
(54) Platz, P. E.; Moheler, J. H. *Biochemistry* **1975**, *14*, 2340.
(55) Cornell, W. D.; Cieplack, P.; Bayly, C. I.; Groud, K. M.; Fergurson, D. M.; Spellmeyer, D. C.; Fox, T.; Cladwell, J. W.; Kollman, P. A. *J. Am. Chem. Soc.* **1995**, *117*, 5179−5197.
(56) Hoover, W. G. *Phys. Rev. A* **1985**, *31*, 1695−1697.
(57) Frisch, M. J.; Trucks, G. W.; Schlegel, H. B.; Scuseria, G. E.; Robb, M. A.; Cheeseman, J. R.; Zakrzewski, V. G.; Montgomery, J. A., Jr.; Stratmann, R. E.; Burant, J. C.; Dapprich, S.; Millam, J. M.; Daniels, A. D.; Kudin, K. N.; Strain, M. C.; Farkas, O.; Tomasi, J.; Barone, V.; Cossi, M.; Cammi, R.; Mennucci, B.; Pomelli, C.; Adamo, C.; Clifford, S.; Ochterski, J.; Petersson, G. A.; Ayala, P. Y.; Cui, Q.; Morokuma, K.; Malick, D. K.; Rabuck, A. D.; Raghavachari, K.; Foresman, J. B.; Cioslowski, J.; Ortiz, J. V.; Stefanov, B. B.; Liu, G.; Liashenko, A.; Piskorz, P.; Komaromi, I.; Gomperts, R.; Martin, R. L.; Fox, D. J.; Keith, T.; Al-Laham, M. A.; Peng, C. Y.; Nanayakkara, A.; Gonzalez, C.; Challacombe, M.; Gill, P. M. W.; Johnson, B. G.; Chen, W.; Wong, M. W.; Andres, J. L.; Head-Gordon, M.; Replogle, E. S.; Pople, J. A. *Gaussian 98*, revision A11.3 Gaussian, Inc.: Pittsburgh, PA, 1998.
(58) Roos, B. O.; Fülscher, M. P.; Malmqvist P-Å.; Merchán, M.; Serrano-Andrés, L. In *Quantum Mechanical Electronic Structure Calculations with Chemical Accuracy*; Langhorff, S. R., Ed.; Kluwer: Dordrecht, The Netherlands, 1994.
(59) Andersson, K.; Barysz, M.; Bernhardsson, A.; Blomberg, M. R. A.; Carissan, Y.; Cooper, D. L.; Cossi, M.; Fleig, T.; Fülscher, M. P.; Gagliardi, L.; de Graaf, C.; Hess, B. A.; Karlström, G.; Lindh, R.; Malmqvist, P.-Å.; Neogrády, P.; Olsen, J.; Roos, B. O. Schimmelpfennig, B.; Schütz, M.; Seijo, L.; Serrano-Andrés, L.; Siegbahn, P. E. M.; Stålring, J.; Thorsteinsson, T.; Veryazov, V.; Wierzbowska, M.; Widmark, P.-O. *MOLCAS*, version 5.2; University of Lund: Lund, Sweden, 2003.
(60) Garavelli, M.; Celani, P.; Bernardi, F.; Robb, M. A.; Olivucci, M. *J. Am. Chem. Soc.* **1997**, *119*, 6891−6901.
(61) González-Luque, R.; Garavelli, M.; Bernardi, F.; Merchán, M.; Robb, M. A.; Olivucci, M. *Proc. Natl. Acad. Sci. U.S.A.* **2000**, *17*, 9379−9384.
(62) Schreiber, M.; Buss, V.; Sugihara, M. *J. Chem. Phys.* **2003**, *119*, 12045−12048.
(63) Schreiber, M.; Buss, V. *Int. J. Quantum Chem.* **2003**, *95*, 882−889.
(64) Page, C. S.; Olivucci, M. *J. Comput. Chem.* **2003**, *24*, 298−309.
(65) Röhrig, U. F.; Guidoni, L.; Rothlisberger, U. *ChemPhysChem* **2005**, *6*, 1836−1847.
(66) During the period of revision of the manuscript, a photoabsorption study of 11-cis Shiff-base retinal chromophore cation in the gas phase has been published: Nielsen, I. B.; Lammich, L.; Andersen, L. H. *Phys. Rev. Lett.* **2006**, *96*, 18304. This study confirms our prediction and places the absorption band due to the optically allowed excitation to the first electronically excited singlet state at around 600 nm.